NUCLEAR INSTRUMENTS AND METHODS 99 (1972) 453–460; © NORTH-HOLLAND PUBLISHING CO.

EQUAL-PATH TIME-OF-FLIGHT NEUTRON DIFFRACTION*

J. M. CARPENTER† and J. D. SUTTON

Department of Nuclear Engineering, The University of Michigan, Ann Arbor, Michigan 48105, U.S.A.

Received 28 June 1971

Measurements of the neutron diffraction patterns of liquids and non-crystalline solids with crystal spectrometer facilities and time-of-flight diffraction techniques are discussed. It is shown that measurements with an equal-path time-of-flight diffractometer generally provide the most accurate representation of a total diffraction pattern. The results of neutron diffraction measurements of vitreous silica with a crystal spectrometer and an equal-path time-of-flight diffractometer are contrasted.

1. Introduction

Neutron diffraction studies of liquids and solids are generally performed with crystal spectrometer facilities. In this paper we contrast the conventional mode of neutron diffraction with time-of-flight diffraction techniques. Particularly, we show the advantages of using equal paths between source and sample and sample and detector in time-of-flight diffractometry.

Due to the motions of the scattering nuclei in a sample, no matter what its physical state – gas, liquid or solid – the scattered intensity distribution contains an inelastically scattered component as well as an elastically scattered part. As a result the measurements must be discussed in terms of the differential scattering cross section

$$\partial^2\sigma(E,E',\theta)/\partial\Omega\,\partial\varepsilon = \sqrt{(E'/E)}\,\mathrm{e}^{-\beta\varepsilon/2}\,S(\varkappa,\varepsilon). \quad (1)$$

$\partial^2\sigma(E,E',\theta)/\partial\Omega\,\partial\varepsilon$ is the differential inelastic scattering cross section per scattering unit in the sample, for neutrons incident at energy E, scattered through angle θ to final energy E'. Since it is convenient for the present purposes, we have introduced the symmetrized scattering law $S(\varkappa,\varepsilon) = S(-\varkappa,-\varepsilon)$. In eq. (1), $E = \frac{1}{2}\hbar^2k^2/m$ is the neutron energy and $\boldsymbol{k}$ the neutron wavevector before scattering. θ is the scattering angle, and $E',\boldsymbol{k}'$ the energy and wavevector after scattering. $\hbar\boldsymbol{\varkappa} = \hbar(\boldsymbol{k}'-\boldsymbol{k})$ is the momentum transfer, $\varepsilon = E'-E$ is the neutron energy gain in scattering, and $\beta = 1/k_{\mathrm{B}}T$.

It is the traditional aim of diffraction measurements to determine the initial value of the Van Hove correlation function, $G(\boldsymbol{r},0)$, through measurements of its Fourier transform, $\Gamma(\boldsymbol{\varkappa})$, the "static structure factor". The exact relationships among $\Gamma(\boldsymbol{\kappa}),G(\boldsymbol{r},0)$ and $S(\boldsymbol{\kappa},\varepsilon)$ are

$$\Gamma(\boldsymbol{\kappa}) = \int \mathrm{d}^3r\,\mathrm{e}^{\mathrm{i}\boldsymbol{\varkappa}\cdot\boldsymbol{r}}G(\boldsymbol{r},0) = \int_{-\infty}^{\infty}\mathrm{d}\varepsilon\,\mathrm{e}^{-\frac{1}{2}\beta\varepsilon}S(\boldsymbol{\kappa},\varepsilon). \quad (2)$$

[The reader is referred for example to the discussion of Lomer and Lowe[1]) for a thorough-going introduction to these principles.]

Due to the inevitable occurrence of inelastic scattering, measurements do not exactly produce the desired static structure factor unless certain conditions are fulfilled. This occurs, namely, only when eqs. (3) and (5) below produce the function $\Gamma(\boldsymbol{\kappa})$ given by eq. (2), as is the case with X-ray diffraction. The effect is widely known, and approaches to overcoming the consequent difficulties of interpreting measurements have been made, theoretically[2]), and experimentally by the method of elastic diffraction[3]), or by integrating the measured scattering law[4]). Here, we discuss another experimental approach to solving this problem, which applies to the method of time-of-flight diffraction. We compare the results of our equal-path time-of-flight diffraction measurements on vitreous SiO_2, with several measurements by Lorch[5,6]).

2. Expressions for the measured intensity distributions

In the conventional measurements made with a crystal spectrometer, as shown schematically in fig. 1, the measured intensity (that is the counting rate) is easily seen to be+

$$I_{\mathrm{c}}(E,\theta) = \phi(E)\Delta E N\int_{E'=0}^{\infty}\mathrm{d}E'\,\frac{\partial^2\sigma}{\partial\Omega\partial\varepsilon}(E,E',\theta)\eta(E')\Delta\Omega, \quad (3)$$

where $\phi(E)$ is the incident neutron flux per unit energy at energy E, ΔE is the interval of selected neutron energies, N is the number of scattering units in the

* This work was supported in part by National Science Foundation Grant GK-1647.

† Present address: Solid State Science Div., Argonne National Laboratory, Argonne, Ill. 60439, U.S.A.

+ For simplicity, we speak here of isotropic systems, such as fluids, powders, and amorphous solids, for which the scattering is independent of azimuthal scattering angle.

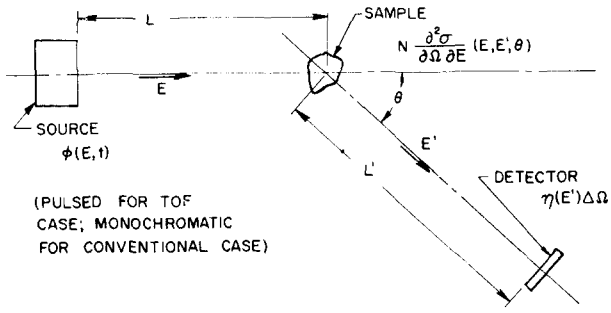

Fig. 1. Schematic representation of a diffraction measurement.

sample, $\Delta\Omega$ is the solid angle subtended by the detector at the sample, and $\eta(E')$ is the detector efficiency for neutrons of energy E'. Most commonly, the intensity is measured as a function of scattering angle θ with a single fixed initial energy E as in a double axis crystal spectrometer.

In measurements made by the time-of-flight method (see also fig. 1), the incident, polychromatic beam is pulsed; the neutrons spread out in time as they travel from the source to the detector, and the intensity distribution is examined as a function of time of flight

$$t = L/v + L'/v', \tag{4}$$

at a fixed scattering angle. L and L' are the flight paths between source and sample, and between sample and detector, and v and v' are the initial and final neutron speeds. For the time-of-flight case, the measured intensity is

$$I_T(t,\theta) = \int_0^\infty dE \int_0^\infty dE' \phi(E)\,\delta\left(t - \frac{L}{v} - \frac{L'}{v'}\right)\Delta t \times N\,\frac{\partial^2\sigma}{\partial\Omega\,\partial\varepsilon}(E,E',\theta)\eta(E')\Delta\Omega, \tag{5}$$

where Δt is the duration of the source pulse. Expressions (3) and (5) account for the fact that neutrons in general scatter inelastically.

When eqs. (3) and (5) are recast in terms of the symmetrized scattering law, the distinctions between what is desired and what is actually measured, become clear. We obtain for conventional diffraction

$$I_c(E,\theta) = N\int_{\varepsilon=-\infty}^{\infty} d\varepsilon W_c(E,\varepsilon)S(\kappa,\varepsilon), \tag{6}$$

where

$$W_c(E,\varepsilon) = \begin{cases} \phi(E)\Delta E\sqrt{\dfrac{E'}{E}}\,\eta(E')\Delta\Omega\,e^{-\frac{1}{2}\beta\varepsilon}, & \text{for } E'>0; \\ 0, & \text{for } E'<0. \end{cases} \tag{7}$$

For time-of-flight diffraction,

$$I_T(t,\theta) = N\int_{\varepsilon=-\infty}^{\infty} d\varepsilon W_T(t,\varepsilon)S(\kappa,\varepsilon), \tag{8}$$

where

$$W_T(t,\varepsilon) = \begin{cases} \phi(E)\Delta E\sqrt{\dfrac{E'}{E}}\,\eta(E')\Delta\Omega\,e^{-\frac{1}{2}\beta\varepsilon}, & \\ & \text{for } E'>\tfrac{1}{2}m(L'/t)^2; \\ 0, & \text{for } E'<\tfrac{1}{2}m(L'/t)^2; \end{cases} \tag{9}$$

where

$$\Delta E = \sqrt{\frac{2}{m}}\,2\,\frac{E^{\frac{3}{2}}}{L}\,\Delta t, \tag{10}$$

$$E = \tfrac{1}{2}m\left[\frac{L}{(t-L'/v')}\right]^2, \tag{11}$$

$$v' = \sqrt{(2E'/m)}. \tag{12}$$

In both eqs. (6) and (8) the scalar momentum transfer is

$$\hbar\varkappa = \sqrt{(2m)}\left[E+E'-2\sqrt{(EE')}\cos\theta\right]^{\frac{1}{2}}, \tag{13}$$

and the energy gain is

$$\varepsilon = E' - E. \tag{14}$$

The integrals (6) and (8) may conveniently be considered as integrations along a path in the $(\varkappa,\varepsilon)$ plane. For conventional diffraction, the instrumental integration path is given by eqs. (13) and (14) with E and θ fixed: for each setting (E,θ) the instrument integrates the product $W_c(E,\varepsilon)S(\varkappa,\varepsilon)$ along that path for $0 \leqq E' < \infty$. In the case of time-of-flight diffraction, the integration path is given by eqs. (13) and (14), with auxiliary eqs. (11) and (12), with t and θ fixed: for each value of (t,θ) the instrument integrates the product $W_T(t,\varepsilon)S(\varkappa,\varepsilon)$ along that path.

The results of measurements are customarily interpreted in terms of the well known static approximation, which can be expressed by

$$S(\varkappa,\varepsilon) \approx \Gamma_{exp}(\varkappa)\delta(\varepsilon). \tag{15}$$

Using this approximation the measurements give a measured structure factor $\Gamma_{exp}(\varkappa_0)$ defined for conventional diffraction, which is given by

$$I_c(E,\theta) = NW_c(E,0)\Gamma^c_{exp}(\kappa_0), \tag{16}$$

where $\hbar\varkappa_0$ is the momentum transfer corresponding to elastic scattering

$$\hbar\varkappa_0 = 2\hbar k_0 \sin\tfrac{1}{2}\theta = (\hbar/\lambda_0)4\pi\sin\tfrac{1}{2}\theta, \tag{17}$$

and k_0 is the incident neutron wavenumber,

$$k_0 = (2mE/\hbar^2)^{\frac{1}{2}} = 2\pi/\lambda_0. \tag{18}$$

For time-of-flight diffraction, interpretation in terms of the static approximation yields the function $\Gamma^T_{exp}(\varkappa_0)$

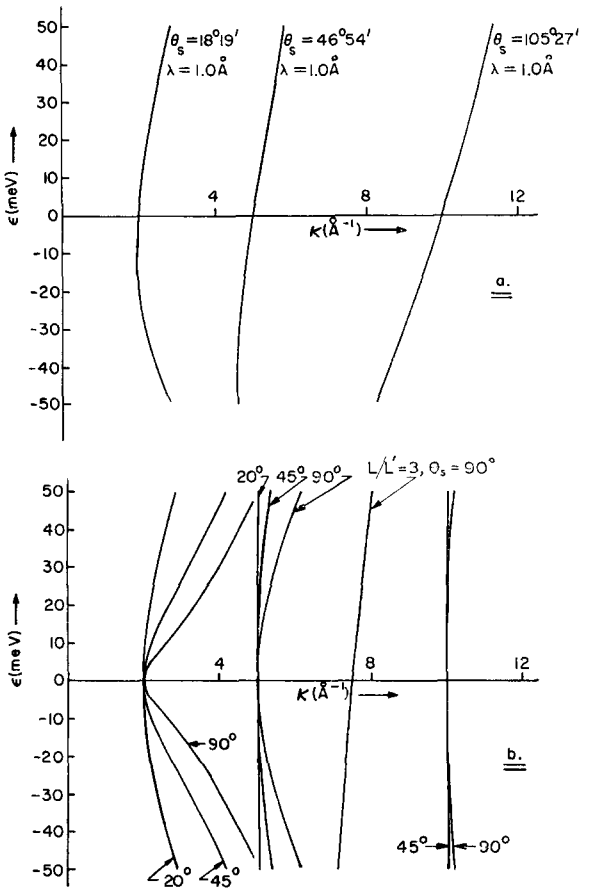

Fig. 2. Instrumental integration paths for (a) crystal diffractometer; (b) time-of-flight diffractometer.

$$I_T(t,\theta) = NW_T(t,0)\Gamma^T_{exp}(\kappa_0), \tag{19}$$

again with the momentum transfer corresponding to elastic scattering where in eq. (17)

$$k_0 = \frac{m}{\hbar}\frac{(L+L')}{t}. \tag{20}$$

The differences between what is measured and the desired static structure factor $\Gamma(\varkappa)$ are of two kinds: a) the instrumental integration of $S(\varkappa,\varepsilon)$ is not along a path of constant $\varkappa$, and b) the integration of $S(\varkappa,\varepsilon)$ is not weighted by the correct function, $\exp(-\frac{1}{2}\beta\varepsilon)$, as required by eq. (2). Below we discuss the two effects separately.

3. Instrumental integration paths

In fig. 2, the instrumental integration paths are shown for several situations. Fig. 2a shows paths for a conventional system, with $\lambda_0 = 1$ Å, which is commonly used. At scattering angles $\theta = 18.3°$, 46.9° and 105.5°, the paths cross $\varepsilon = 0$ at $\varkappa_0 = 2$ Å^{-1}, 5 Å^{-1} and 10 Å^{-1}. Fig. 2b shows paths for the same $\varepsilon = 0$ momentum transfers, for a time-of-flight system. Since it is usually possible to measure at several scattering angles simultaneously, paths are shown which correspond to scattering angles $\theta = 20°$, 45° and 90°, which are easily reached. The paths are shown for the case $L'/L = 1$, and one path is shown for $L/L' = 3$. What is notable is that the instrumental integration paths for the equal flight path time-of-flight cases cross the $\varepsilon = 0$ axis tangent to a constant-$\varkappa$ line. The best time-of-flight paths more nearly approximate the condition of eq. (2) than the paths of the conventional system. The smallest angles provide the closest approach to the constant-$\varkappa$ condition since the neutron energy is then highest.

It is easy to show that in time-of-flight measurements the general condition that the $\varepsilon = 0$ crossover takes place for all $\varkappa$'s at constant-$\varkappa$ (or $\hbar^2\varkappa^2$) is that the flight path lengths L and L' be equal. One wants

$$\left.\frac{d(\hbar^2\kappa^2)}{d\varepsilon}\right|_{\varepsilon=0} = 0. \tag{21}$$

Rewriting eqs. (11) and (12) as

$$f = \sqrt{\frac{2}{m}}\,t - \frac{L'}{\sqrt{E'}} - \frac{L}{\sqrt{E}} = 0, \tag{22}$$

the derivative is easily obtained from the Jacobians*

$$\frac{d(\hbar^2\kappa^2)}{d\varepsilon} = -\left[\frac{\partial(\hbar^2\kappa^2,f)}{\partial(E,E')}\right]\Big/\left[\frac{\partial(\varepsilon,f)}{\partial(E,E')}\right]$$

$$= -\det\begin{pmatrix} \frac{\partial(\hbar^2\kappa^2)}{\partial E} & \frac{\partial f}{\partial E} \\ \frac{\partial(\hbar^2\kappa^2)}{\partial E'} & \frac{\partial f}{\partial E'} \end{pmatrix}\Bigg/ \det\begin{pmatrix} \frac{\partial\varepsilon}{\partial E} & \frac{\partial f}{\partial E} \\ \frac{\partial\varepsilon}{\partial E'} & \frac{\partial f}{\partial E'} \end{pmatrix}. \tag{23}$$

Since $E = E'$ for $\varepsilon = 0$, the derivative is

$$\left.\frac{d(\hbar^2\kappa^2)}{d\varepsilon}\right|_{\varepsilon=0} = 2m\left\{\left[\frac{L'}{E'^{3/2}}\left(1-\sqrt{\frac{E'}{E}}\cos\theta\right)\right.\right.$$

$$\left.\left. - \frac{L}{E^{3/2}}\left(1-\sqrt{\frac{E}{E'}}\cos\theta\right)\right]\Big/\left(\frac{L'}{E'^{3/2}}+\frac{L}{E^{3/2}}\right)\right\}\Bigg|_{E'=E} \tag{24}$$

$$= \frac{2m}{L+L'}(1-\cos\theta)(L-L').$$

The condition that the path intercepts $\varepsilon = 0$ at constant $\varkappa$ for all $\varkappa_0$, is that $L = L'$. It is also easy to see from fig. 2, although we do not prove it here, that the cur-

* See any text on advanced calculus.

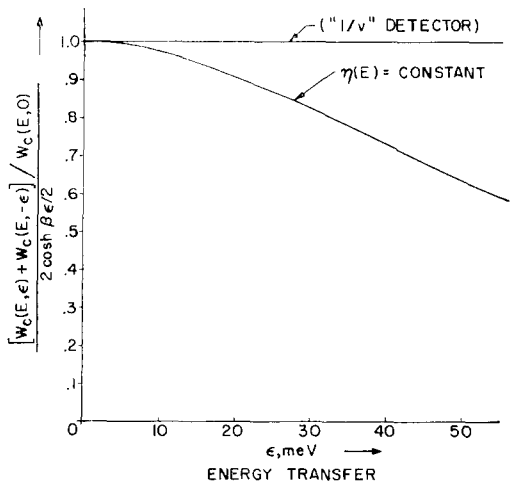

Fig. 3. The ratio of the net normalized weighting function for a crystal diffractometer, to the ideal weighting function. The result is independent of $\varkappa_0$ in the constant-E, variable-θ mode.

vature $d^2\varkappa/d\varepsilon^2|_{\varepsilon=0}$ of the instrumental integration path is minimized when θ is small.

The practical importance of these results is clear: to approximate the condition $\varkappa = \text{constant}$ as nearly as possible, over the largest range of ε along the instrumental integration path, adjust $L = L'$ and choose θ as small as possible in time-of-flight diffraction measurements. The condition that $d\varkappa/d\varepsilon|_{\varepsilon=0} = 0$, cannot be satisfied for conventional neutron diffraction.

It might be thought that the best experimental conditions were reached by choosing the smallest possible L' for given L (or vice versa) so as to accumulate in the same time interval all neutrons scattered from the sample, regardless of their final (or initial) energy. Neither turns out to be the case, as the above analysis shows.

4. Weighting function

Using eqs. (6) and (16), (8) and (19), the measured structure factors can be expressed

$$\Gamma^{c}_{exp}(\kappa_0) = \left[\int_{-\varkappa}^{\varkappa} d\varepsilon W_c(E,\varepsilon)S(\kappa,\varepsilon)\right] \Big/ [W_c(E,0)], \quad (25)$$

and

$$\Gamma^{T}_{exp}(\kappa_0) = \left[\int_{-\varkappa}^{\varkappa} d\varepsilon W_T(t,\varepsilon)S(\kappa,\varepsilon)\right] \Big/ [W_T(t,0)], \quad (26)$$

while the desired structure factor as given by eq. (2) is

$$\Gamma(\kappa) = \int_{-\varkappa}^{\varkappa} d\varepsilon\, e^{-\frac{1}{2}\beta\varepsilon} S(\kappa,\varepsilon). \quad (2)$$

Even given that the path of instrumental integration is a path through $\varepsilon = 0$ at constant-$\varkappa$, the closest approach to a measurement of the desired function is one for which the normalized weighting function $W_c(E,\varepsilon)/W_c(E,0)$ or $W_T(t,\varepsilon)/W_T(t,0)$ most nearly approximates weighting by the function $e^{-\frac{1}{2}\beta\varepsilon}$.

The most important contributions to the integral along the instrumental path come from the region $\varepsilon \approx 0$, since $S(\varkappa,\varepsilon)$ is usually peaked about $\varepsilon = 0$ and decreases more rapidly than $e^{-\frac{1}{2}\beta|\varepsilon|}$ for large $|\varepsilon|$. Therefore, it is of predominant importance that the net weighting functions approximate $e^{-\frac{1}{2}\beta\varepsilon}$ near $\varepsilon = 0$. Taking advantage of the symmetry of $S(\varkappa,\varepsilon)$, we can write the condition that along the instrumental path,

$$\frac{W_c(E,\varepsilon) + W_c(E,-\varepsilon)}{W_c(E,0)} \approx 2\cosh\tfrac{1}{2}\beta\varepsilon, \quad (27)$$

or

$$\frac{W_T(t,\varepsilon) + W_T(t,-\varepsilon)}{W_T(t,0)} \approx 2\cosh\tfrac{1}{2}\beta\varepsilon. \quad (28)$$

The functions $[W(x,\varepsilon) + W(x,-\varepsilon)]/W(x,0)$ might properly be called the "net normalized weighting functions".

Clearly, W_c and W_T are functions peculiar to individual diffractometers, nevertheless, let us consider some realistic cases for a crystal spectrometer, and a time-of-flight diffractometer. For the crystal spectrometer,

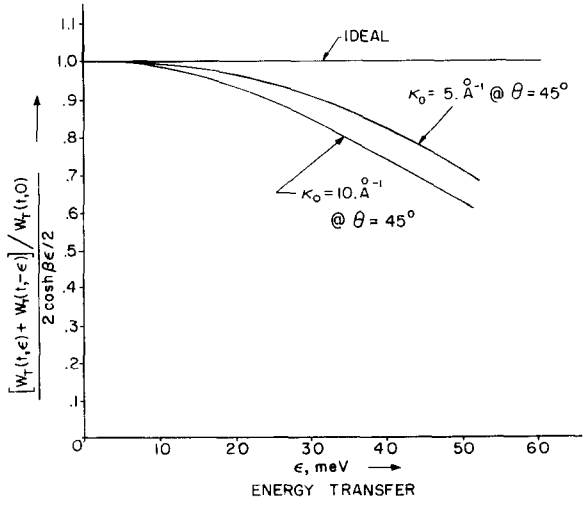

Fig. 4. The ratio of the net normalized weighting function for a time-of-flight diffractometer, to the ideal weighting function. The results are shown for $\varkappa_0 = 5$ Å^{-1} and for $\varkappa_0 = 10$ Å^{-1}.

$$\frac{W_c(E,\varepsilon)+W_c(E,-\varepsilon)}{W_c(E,0)} = \frac{1}{\eta(E)}\left[\sqrt{\left(\frac{E+\varepsilon}{E}\right)}\eta(E+\varepsilon)\,e^{-\frac{1}{2}\beta\varepsilon} + \sqrt{\left(\frac{E-\varepsilon}{E}\right)}\eta(E-\varepsilon)\,e^{+\frac{1}{2}\beta\varepsilon}\right], \quad (\text{for } \varepsilon > -E). \quad (29)$$

The net normalized weighting function is independent of the incident energy spectrum. Assuming a "$1/v$" detector efficiency, eq. (29) gives exactly 2 $\cosh\frac{1}{2}\beta\varepsilon$! For another extreme, a detector of constant efficiency,

$$\frac{W_c(E,\varepsilon)+W_c(E,-\varepsilon)}{W_c(E,0)} = \frac{1}{\sqrt{E}}\left[\sqrt{(E+\varepsilon)}\,e^{-\frac{1}{2}\beta\varepsilon} + \sqrt{(E-\varepsilon)}\,e^{+\frac{1}{2}\beta\varepsilon}\right]. \quad (30)$$

Fig. 3 shows the ratio of this function to the ideal weighting function for $T = 1/k_B\beta = 293$ K, $\lambda_0 = 1$ Å as a function of ε. When the diffractometer is operated in a constant-E, variable-θ mode, the weighting function remains unchanged as $\varkappa_0$ is varied by varying angle θ.

For time-of-flight diffractometers, the net normalized weighting function depends on the incident energy distribution as well as the detector efficiency. Fig. 4 shows the ratio of the net normalized weighting function (eq. 9) to the ideal weighting function, as a function of ε, for a "$1/v$" detector, for sample temperature $T = 293$ K and for a Maxwellian-distributed source

$$\phi(E) = \phi_{Th}\left[\frac{E}{(k_B T_S)^2}\right]\exp(-E/k_B T_S)$$

with effective temperature $T_S = 350$ K, and with a constant Δt. The weighting function varies with $\varkappa_0$. The ratio is shown for paths that intercept the axis at $\varkappa_0 = 5$ Å^{-1} and $\varkappa_0 = 10$ Å^{-1}, appropriate to a scattering angle of 45°.

5. Intensity

Using the following crude argument, it is apparent that the equal-flight-path condition unfortunately gives minimum counting rates. If the source, sample and detector areas are considered to be fixed, then the counting rate is proportional to

$$C \propto \frac{1}{L^2}\cdot\frac{1}{L'^2} = \frac{1}{L^2}\cdot\frac{1}{(L_T-L)^2}, \quad (31)$$

when the total-flight-path length is fixed, $L_T = L + L'$. The function has maxima for $L \to 0$ and $L' \to L_T$, and a minimum value for $L = L' = \frac{1}{2}L_T$. Thus when measurements are made in which intensity is maximized by making either L or L' small, the constant-$\varkappa$ integration path is sacrificed, and the method should be applied only on samples for which the static approximation is well satisfied.

6. Resolution

The question of resolution has no direct bearing on the main results described above. However, to provide a complete albeit abbreviated comparison of the relative merits of conventional and time-of-flight diffraction systems, we present the following simplified analysis. The momentum transfer for elastic scattering is

$$\varkappa_0 = 2k_0 \sin\tfrac{1}{2}\theta. \quad (32)$$

Considering only the contribution to the $\varkappa$ resolution due to uncertainty which arises from angular uncertainties at the scatterer

$$\frac{\delta\kappa_0}{\kappa_0} = \cot\tfrac{1}{2}\theta(\tfrac{1}{2}\delta\theta). \quad (33)$$

Here, $\delta\theta$ is the r.m.s. value of all pertinent angular uncertainties. When θ is varied to change $\varkappa_0$, $\delta\theta$ is approximately constant in the usual experiment.

For time-of-flight diffraction, considering only the contribution to the $\varkappa$ resolution due to uncertainty in $\varkappa_0$ which arises from time-of-flight uncertainties,

$$\frac{\delta\kappa_0}{\kappa_0} = \frac{\delta t}{t}. \quad (34)$$

Here, δt is the r.m.s. value of all pertinent time uncertainties. At different times t which correspond to different $\varkappa_0$, δt remains approximately constant. Fig. 5 shows the resolution $\delta\varkappa_0/\varkappa_0$ for a conventional system operated in the constant-E, variable-θ mode, and a time-of-flight system, according to the above simplifications. Realistic values $\lambda_0 = 1$ Å, $\delta\theta = \frac{1}{3}°$, and $L + L' = 4m$, $\theta = 45°$, and $\delta t = 15$ μsec, have been used in the calculations. The general trend in time-of-flight diffraction is for better resolution at small $\varkappa_0$, and in conventional diffraction, for better resolution at large $\varkappa_0$.

Focusing methods[7]) may still be employed to improve the resolution, even though the condition $L = L'$ is imposed on the diffractometer to achieve the constant-$\varkappa$ integration path.

7. Comparison of conventional with time-of-flight diffraction data on vitreous SiO_2

In the analysis of neutron diffraction by a solid, the problem of correcting measurements of the structure factors for the effects of instrumental integration loci

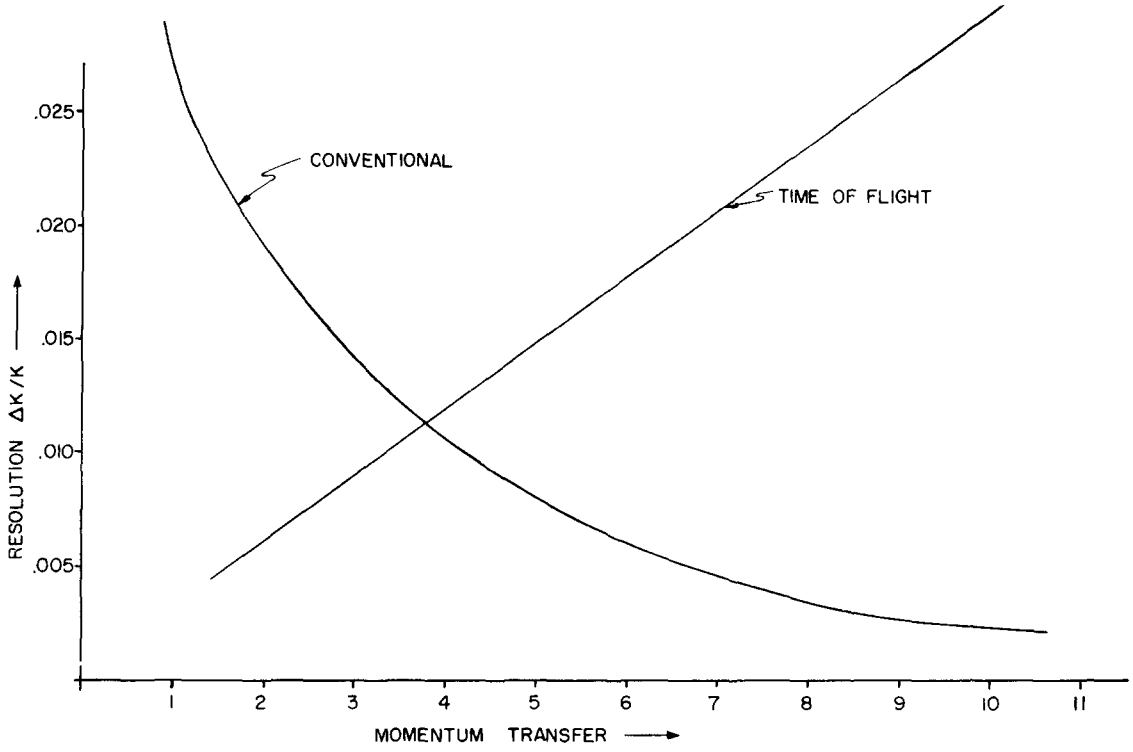

Fig. 5. Representative momentum transfer resolution $\delta\varkappa_0/\varkappa_0$ for (a) crystal diffractometer operated in the constant-E, variable-θ mode; (b) time-of-flight diffractometer.

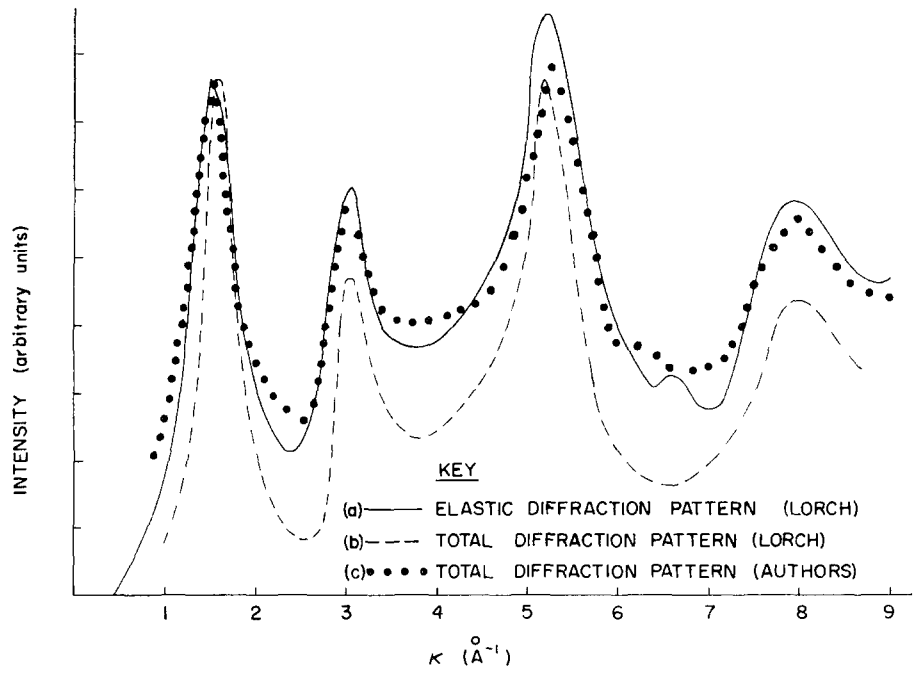

Fig. 6. Static structure factor $I(\varkappa)$ for vitreous silica, as measured by several methods: measurements by Lorch[6]) using (a) elastic diffractometer; (b) conventional crystal diffractometer with $\lambda_0 = 1.13$ Å; (c) measurement by Sutton[8]) using an equal-path time-of-flight diffractometer.

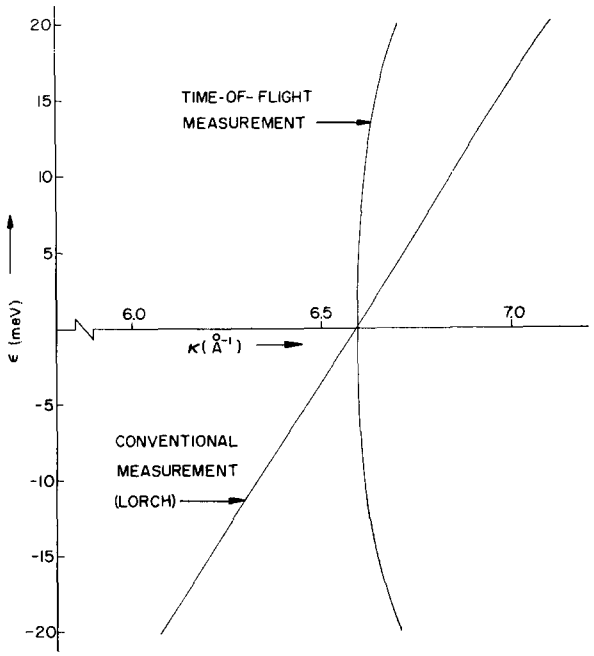

Fig. 7. Instrumental integration paths through $\varkappa = 6.6$ Å^{-1} for the conventional diffractometer used by Lorch with $\lambda_0 = 1.13$ Å and for the equal-path time-of-flight diffractometer.

which do not satisfy the constant-$\varkappa$ condition or for incorrect weighting is seldom considered, for it is generally assumed that the static approximation is valid. However, the results of recent measurements of the neutron diffraction pattern of vitreous silica by Lorch[6]) and some recent measurements of our own[8]) clearly indicate that the diffraction pattern even for this amorphous solid is sensitive to the locus of the measurement in $(\varkappa,\varepsilon)$ space.

Lorch has reported a detailed series of measurements with crystal spectrometer facilities which nicely illustrate the effect of the instrumental integration path and static approximation distortions. His vitreous silica data include measurements of the total diffraction pattern at room temperature (293 K) and liquid nitrogen temperature (77 K) using 1.13 Å wavelength neutrons, a total diffraction pattern at room temperature using 0.75 Å wavelength neutrons, and an elastic diffraction pattern at room temperature obtained with a minimum wavelength of 0.64 Å. The total diffraction pattern measured at room temperature with 1.13 Å neutrons and the elastic diffraction pattern (with Lorch's Debye–Waller correction) are reproduced in fig. 6.

While our fig. 6 reproduces only two of the four measurements discussed by Lorch, we quote his description of his results:

It is immediately apparent that distinct differences occur between the two 1.13 Å [293 and 77 K] patterns. At low $\varkappa$ values the deviations are too small to be observed; however, as the momentum change increases the first deviation is found around the apex (point of large curvature) of the second diffraction peak. After this point deviations are always apparent and seem to reach a maximum around the third diffraction peak which has the sharpest curvature in the whole pattern. It is also noted that the distortions are also asymmetric around this peak.

Except for the region 2–3 Å^{-1} the 0.75 Å curve seems to be intermediate to the two 1.13 Å runs, the most significant feature again being the increased height of the third diffraction peak with respect to that of the first.

In discussing the results of the elastic diffraction measurement, Lorch draws special attention to the small maximum at 6.6 Å^{-1} and notes that no trace of this peak has been found in any previous neutron diffraction measurement.

We have measured the total diffraction pattern of vitreous silica at room temperature with an equal-path time-of-flight diffractometer ($L = L' = 2.1$ m). Our target was a 0.734 cm thick sample of Corning Superpure Vitreous Silica (Code 7940). The measurement is a composite of data taken at scattering angles of 21° and 90°. The intensity of scattering was normalized to an absolute scale by cycling the target with a 0.318 cm thick vanadium target. The experiment included measurements of the total neutron cross section of vitreous silica which were used to correct the diffraction data for the attenuation of singly scattered neutrons in the target and for multiple scattering effects. Resolution in the neighborhood of $\varkappa = 6.6$ Å^{-1} is $\delta\varkappa = 0.2$ Å^{-1} in our data, as shown. The data are shown superimposed on Lorch's results in fig. 6, normalized to equal heights of the first maxima.

Our measurement of the total neutron diffraction pattern of vitreous silica appears more like Lorch's corrected elastic pattern than his total pattern and is the first to indicate the presence of a small feature similar to that which Lorch observes in his elastic diffraction pattern at about 6.6 Å^{-1}. In discussing his results, Lorch comments:

It is difficult to decide whether the appearance of this peak is due to the removal of the static approximation (instrumental integration) distortion or to the fact that $G_e(r)$ is being measured instead of $G(r,0)$. The evidence of X-ray diffraction work (Heaton, 1967) for which the static approximation holds would, however, suggest that the former is the case.

[Lorch alludes to the fact that prominent maxima are observed at $\varkappa \approx 6.6$ Å^{-1} in X-ray diffraction data for vitreous silica[9,10].]

There are several possible reasons why Lorch does not find the 6.6 Å^{-1} feature in his total diffraction data. Since he has used different targets for his total and elastic diffraction measurements, it might be argued that this small feature is strongly sample dependent. However, the X-ray results (and our neutron data) do not support this conclusion. Lorch has also used two different spectrometers for his total and elastic diffraction measurements, and there is no discussion of the relative resolution of the two facilities in his paper. It is our conclusion that the most likely reason that the ≈ 6.6 Å^{-1} feature appears in our total diffraction measurement and not in Lorch's is that the constant-$\varkappa$ condition is more nearly satisfied with the time-of-flight facility. Sample instrumental integration paths for our measurement and Lorch's are shown in fig. 7. One can clearly see that particularly in the small energy transfer region the time-of-flight diffractometer provides a better approximation to the constant momentum transfer condition required for the structure factor measurement. Even though the neutron scattering by vitreous silica is predominantly elastic[8]), it appears that the departure of the crystal spectrometer's measurement locus from the constant-$\varkappa$ condition is sufficient to obscure the presence of the small 6.6 Å^{-1} feature. The comparison illustrates the power of the equal-path time-of-flight diffraction method, in at least one instance where the static approximation would appear to be admirably fulfilled.

References

1) W. M. Lomer and G. G. E. Lowe, in *Thermal neutron scattering* (ed. P. A. Egelstaff; Academic Press, London, 1965).

2) P. Ascarelli and G. Caglioti, Nuovo Cimento [10] **43B** (1966) 375.

3) G. Caglioti, in *Termal neutron diffraction* (ed. B. T. M. Willis; Oxford University Press, London, 1970).

4) J. M. Carpenter and N. A. Lurie, Proc. Symp. *Neutron inelastic scattering*, Copenhagen, 1968, vol. II (IAEA, Vienna, 1969) p. 205.

5) E. Lorch, J. Phys. C (Solid State Phys.) **2** (1969) 229.

6) E. Lorch, J. Phys. C (Solid State Phys.) **3** (1970) 314.

7) K. C. Turberfield, in *Thermal neutron diffraction* (ed. B. T. M. Willis; Oxford University Press, London, 1970); see also, K. F. Graham and J. M. Carpenter, Nucl. Instr. and Meth. **85** (1970) 163.

8) J. D. Sutton, A study of the structure and atomic motions of vitreous silica by thermal neutron scattering methods, Ph.D. Thesis, available from University Microfilms (University of Michigan, Ann Arbor, Michigan, 1971).

9) E. H. Henninger, R. C. Buschert and L. Heaton, J. Phys. Chem. Solids **28** (1967) 423.

10) R. L. Mozzi and B. E. Warren, J. Appl. Cryst. **2** (1969) 164.